





40 potential of (palaeo-)dosimetric or trapped-charge methods, such as Electronic Spin Resonance (ESR) and  
 Optically Stimulated Luminescence (OSL), has been recently explored (e.g. [Gray et al., 2019](#)). While both are  
 extensively used to date Quaternary alluvial environments for instance (e.g. [Rixhon et al., 2017](#)), properties of  
 quartz-luminescence signals have also gained vivid interest for deciphering sediment provenance and sediment  
 transport/mobility in space and time ([Tsukamoto et al., 2011](#); [Gray et al., 2017; 2019](#); [Sawakuchi et al., 2018](#);  
 45 [Mineli et al., 2021](#); [Capaldi et al., 2022](#); [Fitzsimmons et al., 2022](#); [Nelson et al., 2022](#); [Souza et al., 2023](#)). This is  
 particularly true for quartz sensitivity (i.e. the light emitted per unit mass per radiation dose; see e.g. [Pietsch et al.,](#)  
[2008](#); [Sawakuchi et al., 2011a](#); [Fitzsimmons, 2011](#); [Gliganic et al., 2017](#)) which can be acquired using relatively  
 rapid and low-cost measurements compared to conventional provenance-analysis methods (e.g. [Gray et al., 2019](#);  
[Sawakuchi et al., 2020](#)). Similarly, ESR sensitivity (i.e. amount of signal growth per unit dose, [Liu et al 2022](#)) can  
 50 be used to understand the quartz grain history.

Two competing assumptions, however, can explain the variability of quartz sensitivity, making it a matter of  
 current scientific debate. While some argue that it depends on various factors, it is, on the one hand, influenced by  
 the nature and thermal history of the source rock material, making it an intrinsic property of quartz (e.g. [Sawakuchi](#)  
 55 [et al., 2018](#); [Del Rio et al., 2021](#); [Capaldi et al., 2022](#)). On the other hand, it would be induced by surface processes  
 and transport distances, i.e. cycles of erosion-transport-deposition during source-to-sink sediment routing (e.g.  
[Pietsch et al., 2008](#); [Sawakuchi et al., 2011a](#); [Fitzsimmons, 2011](#); [Gliganic et al., 2017](#)). Heat, high pressure,  
 daylight exposure and irradiation during burial can thus all be involved in quartz sensitivity. This conundrum  
 results in three main complications. First, laboratory experiments based on repeated irradiations (i.e. trap filling)  
 60 and bleaching through light exposure (i.e. charge removal) showed somewhat contrasting results for both trapped-  
 charge methods. Whereas OSL sensitisation of quartz occurs over multiple irradiation/bleaching cycles ([Moska &](#)  
[Murray, 2006](#); [Pietsch et al., 2008](#)), possible ESR sensitivity changes under multiple cycles are still debated  
 ([Beerten and Stesmans, 2006](#); [Tissoux et al., 2008](#); [Toyoda et al., 2009](#)). ~~Second~~, quartz-luminescence and ESR  
 analysis for sediment provenance can also be challenging because alluvial sediments typically consist in mixtures  
 65 of countless individual quartz grains and each of them has its own bedrock origin and has undergone its own  
 complex history in a particular catchment area (e.g. [Gray et al., 2019](#)). For this reason, the response of the  
 paramagnetic quartz centres (ESR) or the luminescence sensitivity (OSL) can greatly vary from one alluvial  
 sediment to another, especially in complex geological settings with contrasting natures of quartz-bearing bedrock.  
 Third, quartz grains characterised by low-sensitivity luminescence and ESR signals can be unsuitable for dating  
 70 applications (e.g. [Steffen et al., 2009](#)) and differ between bedrock types and sediment transport history (e.g.  
[Sawakuchi et al., 2011a; 2011b](#)).

Given the complexity of individual sediment grains histories and our insufficient knowledge on the variability of  
 OSL/ESR sensitivities in quartz, one must primarily discriminate whether signal variations are predominantly  
 linked either to the nature of the source material (provenance) or to the sediment history within the catchment  
 75 (sediment dynamics). First, we argue that, before using signals from trapped-charge methods as tracers for  
 sediment dynamics within fluvial routing systems (and improving their full potential for geochronological studies),  
 ESR and OSL signals from source bedrocks must be thoroughly investigated. Except a handful of studies over the  
 two last decades ([Sawakuchi et al., 2011a](#); [Jeong and Choi, 2012](#); [Zular et al., 2015](#); [Guralnik et al., 2015](#)), this  
 key part of the question was clearly disregarded. This is all the more problematic as quartz formed under distinct



80 conditions (e.g. plutonic versus metamorphic processes or magma of various compositions) will contain different number and nature of luminescent and/or paramagnetic centres, leading to distinct ESR and OSL responses. Second, if a correlation between the ESR/OSL sensitivity and trace-element contents in quartz was suggested, only few studies quantitatively explored these potential chemical/physical relationships (e.g. [Usami \(2010 in Shimada et al., 2016\)](#)). Third, physical relationships between ESR paramagnetic centres and OSL luminescent centres were 85 proposed (e.g. [Preusser et al., 2009](#)) yet insufficiently explored.

Against this background, this study primarily aims to understand how each quartz grain/aliquot holds a source-specific signature by investigating variability in primary ESR and OSL characteristics related to different bedrock nature, composition and history. We thus focus on quartz grains originating from magmatic, metamorphic and sedimentary formations occurring in a small-sized catchment (the so-called Strengbach) draining the Variscan 90 Vosges Massif located in easternmost France. Both ESR and OSL measurements are performed alongside with trace element determination by mass spectrometry coupled to laser ablation (LA-ICPMS). We specifically emphasise on Al, Li, and Ti contents because they are (i) some of the most common trace elements in quartz, (ii) the primary paramagnetic centres used in ESR dating, and (iii) suspected to closely control OSL signal sensitivity. Such systematic comparison between ESR and OSL luminescence characteristics, in relation to trace element 95 content in quartz, is unique and our results highlight the potential of combining physical and chemical quantitative approaches to assess sediment provenance in natural geological systems. These results may have future implications in tracing sediment dynamics and provenance, but also in dating Quaternary alluvial sediments derived from various bedrock types in complex geological environments.

## 2 Overview of OSL and ESR methods as sediment/bedrock tracers

### 100 2.1 OSL sensitivity on primary source bedrocks

Reported values of OSL sensitivity in quartz ranges from two to five orders of magnitude between crystalline rocks (magmatic and metamorphic) and sedimentary rocks ([Alexanderson, 2022](#); [Mineli et al., 2021](#); [Sawakuchi et al., 2011a, 2020](#); [Souza et al., 2023](#)). This large variability was linked to magma-crystallisation processes and/or pressure-temperature conditions during metamorphism ([Lukas et al., 2007](#); [Sawakuchi et al., 2011](#); [Jeong and 105 Choi, 2012](#); [Zular et al., 2015](#); [Guralnik et al., 2015](#)). Higher OSL sensitivity observed in quartz-bearing bedrock formed at high temperatures probably results from crystallization temperature on the production of intrinsic or extrinsic defects in quartz ([Sawakuchi et al., 2011b](#)). Higher crystallization temperature favours both key processes at the heart of the luminescence phenomenon in quartz by increasing the occurrence of Si- and O-vacancies ([Preusser et al., 2009](#)) and the substitution of  $\text{Si}^{4+}$  cations by  $\text{Al}^{3+}$  and  $\text{Ti}^{4+}$  ([Dennen et al., 1970](#); [Götze et al., 2001](#); 110 [Wark and Watson, 2006](#)). Laboratory experiments also report increasing luminescence sensitivity in quartz with heating ([Bøtter-Jensen et al., 1995](#); [David and Sunta, 1981](#); [Koul, 2006](#); [Polymeris et al., 2007](#); [Poolton et al., 2000](#); [Rink et al., 1993](#)).

On the other hand, both sensitisation of quartz and presence of a fast component signal are supposed to increase with sediment transport distance and the number of burial-exposure cycles ([Pietsch et al., 2008](#); [Fitzsimmons, 115 2011](#); [Rhodes and Pownall, 1994](#); [Preusser et al., 2006](#); [Lukas et al., 2007](#); [Gray et al., 2019](#)), as documented by laboratory experiments with repetitive irradiation-bleaching treatments ([McKeever et al., 1996](#); [Li, 2002](#); [Moska and Murray, 2006](#); [Koul and Chougankar, 2007](#)). Thus, low sensitivity of quartz grains is commonly attributed



to minimal transport distance and/or young sedimentary history. By contrast with bright OSL signals measured in highly reworked sediments, primary source bedrocks contain dim quartz grains characterised by low OSL sensitivities and almost no fast component, making them very difficult to use as only few grains provide a luminescence signal (Sawakuchi et al., 2011a; Jeong and Choi, 2012; Guralnik et al., 2015; Mineli et al., 2021). It may be also indicative of different intrinsic concentration of holes at certain light-sensitive recombination centres and types of impurities and defects in the mineral structure, which control the main luminescence traps and centres (Preusser et al., 2006, 2009).

## 2.2 ESR characteristics on primary source bedrocks

ESR spectra linked to Al and Ti paramagnetic centres traditionally measured in quartz aliquots for dating studies (Ikeya, 1993) document large variabilities related to the saturation value or the Ti/Al intensities ratios. Interestingly, geographical provenance of quartz, likely in relation with the regional bedrock geological nature, seems playing a key role here with variable configurations: high intensities for both centres (e.g. USA, Indonesia, Toyoda et al., 1994; Appendix A) or high intensity for one centre only, including (very) high Al versus weak (or even absent) Ti intensity in the Pyrenees foreland (Delmas et al., 2018) and Chinese loess (Toyoda, 2015), or the opposite (e.g. Philippines; Ingicco et al., 2018). Moreover, the very few existing studies on primary source bedrocks mainly focused on the non-radiosensitive E1' centre of quartz (i.e. O-vacancy electron centre). As it may act as a non-radiative centre competing with the recombination process (Poolton et al., 2000), it is not used for dating applications (e.g. Jani et al., 1983; Toyoda and Ikeya, 1991; 1994; Ono et al., 1998; Toyoda et al., 2016). However, Duttine et al. (2003) and Kotova et al. (2008) highlighted some differences between the relative intensities of Ge, Al and Ti paramagnetic centres in different bedrocks ( $[\text{GeO}_4/\text{Na}^+]^\circ$ ,  $[\text{GeO}_4/\text{Li}^+]^\circ$ ,  $[\text{AlO}_4/\text{h}]^\circ$ ,  $[\text{TiO}_4/\text{H}^+]^\circ$ ,  $[\text{TiO}_4/\text{Li}^+]^\circ$ ,  $[\text{TiO}_4/\text{Na}^+]^\circ$ ). Moreover, Shimada et al.'s (2013) study on the E1' centres in relation to signal intensity of Al and Ti-Li in quartz from various Japanese bedrocks and sedimentary deposits showed distinctions between volcanic and granitic sources, thereby suggesting that ESR signals in quartz may be used as a source tracer. In addition, intensity ratios of Al, Ti-Li or Ti-H centres in quartz grains from various river sediments can be related to provenance in the catchment (Tissoux et al., 2015; Shimada et al., 2016). Whilst the influence of grain-size on the ESR response of quartz was thoroughly studied (Timar-Gabor, 2018), comparable results can only be obtained using samples of similar grain-size fractions (Shimada et al., 2016).

## 3 Study area and sampling

The Strengbach catchment is located in easternmost France and drains the western flank of the Vosges Massif (Fig. 1a). This low mountain range is part of the Variscan orogen that formed during the subduction and subsequent collision of the Saxothuringian plate below the Moldanubian plate during the second half of the Palaeozoic (Schulmann et al., 2014). This specific catchment was selected because of two main reasons. First, hydrological, hydrogeological and (hydro-)geochemical monitoring has been continuously achieved in the catchment's headwaters over more than 30 years with quantitative data on *in situ* silicate dissolution (e.g. Wild et al., 2019), including quartz, together with regolith evolution on millennial timescale (Ackerer et al., 2016). Second, despite the catchment's small size (<40 km<sup>2</sup>), it hosts various quartz-bearing lithologies, including Palaeozoic



155 metamorphic and plutonic rocks and Mesozoic sedimentary rocks (Fig. 1b). All of them were sampled and are presented hereinafter in detail in chronological order.

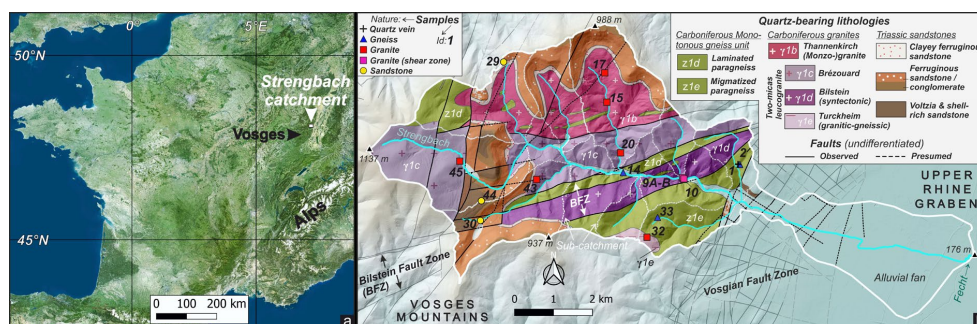


**Figure 1: a) Location of the study area in the Vosges; b) geological map of the Strengbach catchment, adapted and simplified from the French Geological Survey's (BRGM) geological map.**

### 160 3.1 Metamorphic basement

The metamorphic basement covers ca. 20% of the drainage area. It is composed of sillimanite paragneiss from the so-called Monotonous Gneiss Unit (von Eller, 1961). The latter formed during the Carboniferous from late Cambrian-early Ordovician sediments (Skrzypek et al., 2012) under a medium pressure and temperature conditions prograde metamorphism followed by a near isothermal decompression associated with rapid exhumation (Latouche et al., 1992; Rey et al., 1992; Schulmann et al., 2002). Spatial variations occur within the Monotonous gneiss facies linked to the gneiss protolith and later evolution involving fracturing, magmatic and hydrothermal activity. In particular, gneissic units to the South of the Bilstein fault zone are affected by an increasing degree of partial melting materialised by the transition to migmatitic domains to the south of the watershed (z1e, Fig. 1b; Fluck et al., 1991; von Eller, 1961).

### 170 3.2 Granitic intrusions

Four different Carboniferous leucogranites cover ca. 50% of the drainage area and intrude the metamorphic basement along major faults, such as the Bilstein fault zone (BFZ) in the Strengbach catchment (Fig. 1b; Fluck et al., 1991; Skrzypek et al., 2014). They match one of the latest magmatic events during the Vosges Massif's formation which occurred during a phase of N-S extensional subsidence of the orogen ca. 10-15 Ma after the metamorphic basement's rapid exhumation (Skrzypek et al., 2014; Tabaud et al., 2014). The so-called Thannenkirch granite (γ1b) first intruded the basement (Kratinova et al., 2007). It is a porphyroid, biotite-rich anatectic monzogranite that formed from the melting of the surrounding gneiss (von Eller, 1961). The so-called Brézouard (γ1c), Bilstein (γ1d) and Turckheim (γ1e) granites subsequently formed from melting of deeper crustal material (Fluck et al., 1991; von Eller, 1961). The Brézouard granite was second to intrude the basement, followed by the syntectonic Bilstein granite (Kratinova et al., 2007). The Bilstein granite formed while the BFZ was active and deformed following a ca. N70 sinistral motion (von Eller, 1961). Such deformation can also be found in the southern part of the Brézouard pluton and within the Thannenkirch pluton (Fluck et al., 1991; Kratinova et al., 2007). Within the Thannenkirch pluton, the so-called Verreries facies hosts granito-gneissic features as the anatectic fusion remained in an early stage (von Eller, 1961). The Turckheim granite only marginally intrudes the



185 Monotonous Gneiss Unit to the south of the Strengbach catchment. While its relative formation timing remains  
 unknown, it locally evidences granito-gneissic characteristics (Blanat et al., 1972).

### 3.3 Sedimentary cover

190 Triassic Buntsandstein units (mostly sandstones) are deposited on top of crystalline rock formations, following the  
 intrusion of various leucogranites during the Carboniferous and a long-lasting erosional episode materialised by a  
 ca.50 Ma hiatus in the geological record. Three preserved units cover ca. 25% of the Strengbach's drainage area  
 (Fig. 1b). The lower one is the Vosgian basal unit (t1a) made of clayey ferruginous sandstone (lower  
 Buntsandstein). The intermediate and main one (t1-2V & 2P) matches undifferentiated Vosgian sandstone and  
 conglomerate (lower to upper Buntsandstein). The upper one (t2-3 & t3c) is made of Voltzia and shell-rich  
 sandstone (upper Buntsandstein to lower Muchelkalk). Whereas fluvial depositional environments are traditionally  
 195 attributed to the two lower units, the upper one is related to a deltaic environment (Gall, 2006). The subsidence of  
 the Upper Rhine Graben (mostly Cenozoic) led to the formation of major N-S oriented faults that crosscut the  
 westernmost part of the Strengbach catchment (von Eller, 1961).

### 3.4. Sampling strategy

200 The Strengbach catchment's small size (ca. 40 km<sup>2</sup>) and easy access to source material both enabled systematic  
 sampling of all quartz-bearing rock formations. Altogether, fifteen bedrock samples were collected throughout the  
 catchment (Fig. 1b, Table 1, Appendix B). Three of them were collected from the Monotonous gneiss unit: one in  
 each facies that are laminated (Z1d, #14) and migmatized (z1e, #02) paragneisses (i.e. "Gneiss") along with one  
 metamorphic quartz vein sample (#01; i.e. "Vein"). Nine granitic samples form the bulk of our dataset as this  
 lithology roughly constitutes the half of the drainage area: Three samples were collected in the Bilstein granite  
 205 (γ1d, #9A, 9B and 10) close to a shear zone (i.e. "Deformed granite"). Six granites were collected from intrusions  
 (γ1b and γ1c #15, 17, 20, 45; i.e. "Granite") and (γ1e, #32, 33; i.e. "Altered granite"). The remaining three samples  
 (#29, 30, 44) were collected from the Triassic Buntsandstein formations, i.e. one sample per sedimentary unit (t1a,  
 t1-2V & 2P and t2-3 & t3c; i.e. "Sandstone"). Table 1 summarises the sampled rock formations with labels, ages  
 and a short description of lithology and conditions of formation.

210

Bedrock unit and ID <sup>a</sup>	Rock description <sup>b</sup>	Conditions of formation <sup>c</sup>	Chronology	Sample ID
Monotonous gneiss unit - z1d	Laminated sillimanite paragneiss	PT conditions of ~6-7 kbar and 600-660 ± 50°C	Carboniferous (older than granites)	14
Monotonous gneiss unit - z1e	Migmatized sillimanite paragneiss	PT conditions of ~4 kbar and 640 ± 80°C	Carboniferous (older than granites)	1 <sup>d</sup> , 2
Thannenkirsch granite - γ1b	Biotite porphyroid anatectic monzogranite	Cooling around 600°C	Carboniferous 314 ± 9 Ma* 326 ± 1 Ma**	15
Thannenkirsch granite (Verreries facies) - γ1b	Thannenkirsch granite with granito-gneissic features		306.6 ± 6.2 Ma***	17
Brézouard granite - γ1c	Two-micas leucogranite	Cooling around 500°C	Carboniferous 323 ± 10 Ma* 329 ± 2 Ma** 332 ± 8 Ma*** 307 Ma****	20, 45





Bilstein granite - $\gamma 1d$	Two-micas syntectonic leucogranite	Cooling around 350-400°C	Carboniferous 323 $\pm$ 10 Ma* 323 $\pm$ 10 Ma** 334 $\pm$ 2.4 Ma*** 335 Ma****	9A, 9B, 10
Turckheim granite - $\gamma 1e$	Two-micas leucogranite with granito-gneissic features	Cooling around 500°C	Carboniferous	32,33
Vosgian sandstone basal unit - t1a	Clayey ferruginous sandstone	Deposition in a fluvial environment	Triassic (lower Buntsandstein)	29
Undifferentiated Vosgian sandstone and conglomerate - t1-2V & 2P	Coarse ferruginous sandstone and conglomerate	Deposition in a fluvial environment	Triassic (lower to upper Buntsandstein)	30
Sandstones - t2-3 & t3c	Voltzia and shell-rich sandstone	Deposition in a deltaic environment	Triassic (upper Buntsandstein to lower Muchelkalk)	44

**Table 1: Main characteristics of rock formations sampled for ESR analysis in the Strengbach catchment. a) referring to BRGM 1:50 000 map & notice; b) after von Eller (1967), Fluck (1980), and Saavedra et al.(1973); c) Metamorphic PT conditions and depositional environments; d) quartz vein sampled in metamorphic rock formations Dating methods: \* K-Ar – chlorite or muscovite (data from Boutin et al., 1995); \*\* U-Pb – zircon (data from Kratinová et al., 2007 and Schulmann et al. 2002); \*\*\* Ar-Ar – muscovite or amphibole (data from Boutin et al., 1995); \*\*\*\* Rb-Sr – muscovite and bulk (data from Bonhomme, 1967)**

## 4 Methods and protocol

### 4.1 Sample preparation

220 Bedrock samples were prepared and processed at the OSL laboratory of the *Centre de Recherche et d'Enseignement des Géosciences de l'Environnement* (CEREGE, Aix en Provence, France). For each bedrock sample, between ~1 and 4 kg of rocks were gently crushed and sieved to isolate the 180-250  $\mu\text{m}$  grain-size fraction, followed by a first chemical bath with 37% HCl to remove potential surface carbonates, followed by magnetic separation with a Frantz magnetic separator (two steps at 10°-0.5A and 10°-1.5A) to remove magnetic and/or heavy minerals. Following this separation, ~50 to 70 g of the remaining material undergone chemical treatment for a week with a slight stirring in a solution of 1/3 of HCl and 2/3 of  $\text{H}_2\text{SiF}_6$  to remove a large part of the feldspar grains. Density separation using lithium heteropolytungstate (LST) heavy liquid at 2.62  $\text{g/cm}^3$  density was performed to further isolate quartz from feldspar. If feldspar grains were still detected under the binocular magnifier, we performed a second magnetic separation with addition of magnetite powder, followed by a rinsing step in a solution of 10% of HCl. No HF treatment was performed for preserving as much as possible the quartz-grain structure and surface for future analyses such as trace-element distribution with Laser Induced Breakdown Spectroscopy (LIBS). This step was replaced by a second treatment for a week in a solution of 1/3 of HCl and 2/3 of  $\text{H}_2\text{SiF}_6$  to remove any remaining feldspar inclusions. Finally, the prepared samples were separated into two batches to be measured by ESR and OSL. In parallel, 100  $\mu\text{m}$  thick sections of each rock were created for analysis by Laser ablation inductively coupled mass spectrometry (LA-ICPMS).



## 4.2 OSL measurements and sensitivity analysis

Aliquots of ~100-300 quartz grains were mounted in stainless discs using silicon oil, and a first evaluation of feldspar contamination was performed using infrared (IR) stimulation at 60°C before further analysis. Luminescence signals were measured on stainless plates using a Leksygs smart reader equipped with a beta radiation source delivering a dose rate of ~0.124 Gy/s, with blue (458 nm, maximum power of 100 mW/cm<sup>2</sup>) and infrared (850 nm, maximum power of 200 mW/cm<sup>2</sup>) LEDs for stimulations and filters (Hoya-U340 + Delta-BP 365/50) for light detection in the ultraviolet band.

Luminescence measurements for OSL at 125°C and TL sensitivities were carried out following the protocols modified from Sawakuchi et al. (2020) or Mineli et al. (2021), which are presented in Table 2. For each bedrock sample, three aliquots were measured and subsequently weighted for mass normalisation.

The aliquots were first bleached for 300 s at 90 mW/cm<sup>2</sup> and 125°C before any given dose. Then, a given dose of 50 Gy was given to all aliquots to allow, along with mass normalisation, uniform inter-comparisons of the measured luminescence signals among samples. In a first experiment, the TL peak of quartz at 110°C (Murray and Roberts, 1998) is investigated to evaluate its natural sensitivity and possible correlation with the OSL sensitivity.

The TL peak is calculated by integrating the TL signal between 75 and 125°C (TL<sub>110°C</sub>), normalized by the given dose and the aliquot mass (photon cts /Gy/mg). After IR stimulation at 60°C to confirm the quartz purity of the aliquot, the OSL sensitivity is measured using blue light stimulation at 125°C (BOSL<sub>125°C</sub>) and corresponds to the counts integrated over the first second of light emission, minus the normalised background from the last 10s of the OSL decay curve. In a second experiment (treatment B in Table 2), we evaluate the quartz OSL sensitivity after a second similar irradiation dose but measured at room temperature (BOSL<sub>25°C</sub>), which corresponds to the integral of the first second of light emission, minus the late background. Both signals are also normalized by the given dose and the aliquot mass (photon cts /Gy/mg).

Step	Treatment A	Observed A	Treatment B	Observed B
1	Blue LED stimulation at 125°C for 300 sec	Bleach	Blue LED stimulation at 125°C for 300 sec	Bleach
2	Given dose, 50 Gy	Irradiation	Given dose, 50 Gy	Irradiation
3	TL up to 190°C for 10 sec	<b>110°C TL sensitivity</b> [75-125°C]	IR LED stimulation at 25°C for 300 sec	IRSL
4	IR LED stimulation at 60°C for 300 sec	<b>IRSL</b>	Blue LED stimulation at 25°C for 100 sec	OSL sensitivity <b>BOSL<sub>f</sub> 25°C</b> [1 sec OSL - BG]
5	Blue LED stimulation at 125°C for 110 sec	OSL sensitivity ( <b>BOSL<sub>f</sub> 125°C</b> ) [1 sec OSL - BG]	Blue LED stimulation at 125°C for 100 sec	OSL sensitivity <b>BOSL<sub>f</sub> 125°C</b> [1 sec OSL - BG]
6	Blue LED stimulation at 125°C for 300 sec	Background		

Table 2: Analytical protocol to measure the TL peak at 110°C and BOSL at 125°C (columns A), adapted from Sawakuchi et al. (2020) and to measure the BOSL sensitivity at 25°C (columns B), adapted from Mineli et al. (2021). Data considered in this article are shown in bold





### 4.3 ESR measurements

Measurements by ESR spectrometry imply the separation of all samples into two aliquots weighing ~100 mg each. One aliquot of each sample was exposed to light (SOL2 solar simulator - HONLE) for 2000 hours (Toyoda et al., 2000) to achieve maximum bleaching of Al and Ti ESR centres. Both bleached and natural (non-bleached) aliquots were then measured in an EMX Bruker ESR spectrometer located in the laboratory of Histoire Naturelle de l'Homme Préhistorique (Paris, France) using following parameters: 5 mW microwave power; temperature of 90°K; 1024 point resolution; 20 mT sweep width; 100 kHz modulation frequency; 0.1 mT modulation amplitude; 40 ms conversion time - 20 ms time constant. The Al, Ti-Li and Ti-H centres were measured simultaneously following Toyoda and Falguères's (2003) recommendations for the Al centre and those of Toyoda et al. (2000) for Ti centres. ESR intensities were measured for all centres and provided following information: (i) the total intensity of the Al centre from the natural aliquot (Al), (ii) the optically non-bleachable intensity of the Al centre (DAT) corresponding to the intensity of the bleached aliquot; (iii) the OBAT: Optically bleachable intensity of the Al centre (OBAT) obtained by  $(Al) - (DAT)$ , (iv) the bleaching rate of the Al centre (BI%) obtained by  $((Al-DAT)/Al) * 100$ , the Ti-Li intensity (Ti-Li) and the Ti-H intensity (Ti-H). We reasonably assume that both Al and Ti centres have reached saturation before sample processing and measurements because source bedrocks are older than 250 Ma.

### 4.4 LA-ICPMS analyses

LA-ICPMS analyses were performed in the laboratories of the French Geological Survey (BRGM, Orléans, France) on an Agilent 8900 Triple Quadrupole ICP-MS coupled to a 193 nm Teledyne CETAC Technologies Photon-Machine Excite Excimer laser equipped with a HelEx 2 laser-ablation cell. The laser was run at a shot frequency of 8 Hz, energy was set to 6 mJ, and a spot size of 50  $\mu$ m was used. The acquisition of each spot lasted 60 seconds with 20 seconds of background before the start of the 30-second-long ablation. To prevent quartz from breaking under the laser beam, analyses were carried out on thick sections made from whole rock samples from bedrocks. A total of fifteen samples were analysed for trace elements in quartz (including Al, Li, and Ti) with between 28 and 60 spots on the various quartz grains present on the thick section. Element concentrations were obtained from the raw data using the software Glitter. Nist 612 was used as external standard (Pearce et al., 1997) and a concentration of 99.9% SiO<sub>2</sub> was used as internal standard for quantification. Data are based on a background-subtracted-signal. Signal smaller than three times the background noise standard deviation was excluded, and detection limits were calculated based on these criteria for each analysis. Commonly, the highest calculated detection limit of each analysed element is selected and used to further exclude any data lower than these values. This is done so that the dataset is consistent and comparable. However, in our case, this implies the exclusion of an important number of otherwise reliable data (i.e. all Li concentrations of sample STR22-33). We decided instead to keep values for all the analyses that were above their associated limit of detection and to provide the maximum LOD for each sample as an indicator. Values below or close to the maximum LOD of each sample should be considered as indicative values rather than exact values. The median concentration for each considered element was calculated for each sample to allow comparisons with ESR and OSL data (i.e. aliquots with several hundreds of grains). The estimation error is defined as the half of the interquartile range. Tables with detection limits and median values per sample are provided in the supplementary information (Appendix C).



## 300 5 Results

### 5.1 OSL and ESR measurements

First, sensitivity values related to  $BOSL_{125^{\circ}C}$  measurements range from ~10 to ~250 cts/Gy/mg. This variability together with an OSL sensitivity gradient allow distinguishing two categories of bedrocks including eight and seven samples, respectively. On the one hand, low sensitivities ranging from 10 to 60 cts/Gy/mg are found in the quartz vein (z1d; #01), both gneisses (z1d-e; #02, 14) and the syntectonic Bilstein granite ( $\gamma$ 1d; #9A-B, 10) along with the gneissic Turckheim granite ( $\gamma$ 1f; #32, 33). On the other hand, both remaining granites ( $\gamma$ 1b; #15, 17 and  $\gamma$ 1c; #20, 45) along with all Triassic sandstones (t1a, t1-2 and t2-3; #29,30, 44) present much brighter signals comprised between 100 and 250 cts/Gy/mg. The highest sensitivity is observed in the lower Triassic sandstone (#29), which also shows a higher variability in measured aliquots. Second, Third,  $TL_{110^{\circ}C}$  peak sensitivities present a pattern similar to that observed for the  $BOSL_{125^{\circ}C}$ , with values ranging from ~270 to 3300 cts/Gy/mg. The highest  $TL_{110^{\circ}C}$  sensitivity values are documented for granites and sandstones, the same sandstone sample (#29) as before showing much higher values than other bedrock samples. Third, sensitivity values related to  $BOSL_{25^{\circ}C}$  measurements follow the same pattern with two groups of low and high  $BOSL_{25^{\circ}C}$  intensities including the same lithologies as before. Comparison between  $BOSL_{25^{\circ}C}$  and  $BOSL_{125^{\circ}C}$  signals show an excellent linear correlation ( $R^2=0.893$ ) so that the different bedrock types plot along this linear fitting trend (Fig.2A). A good linear correlation is also observed between  $TL_{110^{\circ}C}$  and  $BOSL_{125^{\circ}C}$  ( $R^2=0.647$ ,  $R^2=0.804$  without #32 outlier; Fig.2B).

Optically unbleachable (DAT) and Optically bleachable (OBAT) intensities of the Al centres along with Ti-Li and Ti-H intensities of each sample were measured on the same aliquot. The OBAT vs DAT (Fig.2C) are extremely variable between bedrock. First, main bedrock types (i.e. plutonic, metamorphic and sedimentary) clearly cluster into sub-groups, with the quartz vein (#01) clearly plotting apart (Fig.2C). The latter also shows the lowest DAT intensities whereas the highest values are reported in the Bilstein deformed granites (#09A, 09B, 10). OBAT intensities display similar results: lowest value for the quartz vein vs highest values for all types of granites. Second, the comparison between Ti-Li and Ti-H intensities shows a linear correlation ( $R^2=0.874$ ; Fig. 2D). It allows distinguishing two groups of bedrocks, similar to those based on  $BOSL_{125^{\circ}C}$  measurements: low Ti-Li and Ti-H intensities for the quartz vein, gneisses and the Bilstein granite vs high Ti-Li and Ti-H intensities for all remaining granites and sandstones. Given this excellent correlation between Ti-Li and Ti-H intensities, only the former will be discussed in the following since our conclusions made on Ti-Li are considered as effective also for Ti-H. Third, intensity comparison of Al vs Ti-Li shows no linear correlation. Whereas most of the Al values cluster around ~600 a.u., Ti-Li intensities scatter between 0 and 60 a.u (Fig 2E).

The comparison between  $BOSL_{125^{\circ}C}$  sensitivities and Ti-Li intensities highlights two distinct groups: low sensitivities/intensities for the quartz vein, gneisses and Turckheim and Bilstein granites vs high sensitivities/intensities for the remaining granites and sandstones (Fig. 2F) However no significant relationship can be calculated ( $R^2<0.5$ ). Sample #32 plots apart. By contrast, comparison of  $BOSL_{125^{\circ}C}$  sensitivities with Al intensities shows no linear correlation as the latter cluster around 600 a.u. and 900 a.u. (Fig.2G). We noticed that depending on the type of measurements, sample #32 shifts within bedrock groups: its  $BOSL_{125^{\circ}C}$  sensitivity and ESR-Al intensity are similar to gneisses, while its ESR Ti-H and Ti-Li intensities place it in the granites/sandstones group.

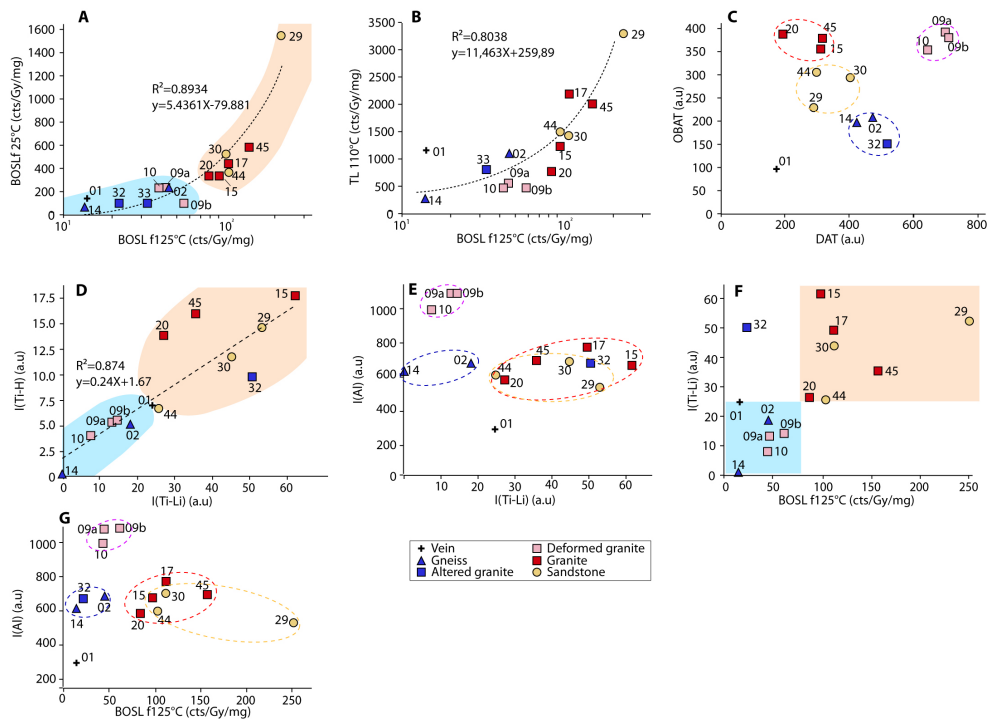


Figure 2: Graphical representations of the data obtained by ESR, OSL on quartz grains extracted from magmatic, metamorphic and sedimentary rocks in the Strengbach basin. ESR Intensities or OSL sensitivities plotted : A) BOSL<sub>25°C</sub> vs BOSL<sub>125°C</sub>; B) TL<sub>110°C</sub> vs BOSL<sub>125°C</sub>; C) ESR Al OBAT vs ESR Al DAT; D) ESR Ti-H vs ESR Ti-Li; E) ESR Al vs ESR Ti-Li; F) ESR Ti-Li vs BOSL<sub>125°C</sub>; G) ESR Al vs BOSL<sub>125°C</sub>

## 5.2 Trace element content

Al, Ti and Li concentrations are in the order of a hundred ppm for Al and around ten ppm for Ti and Li (Fig 3).

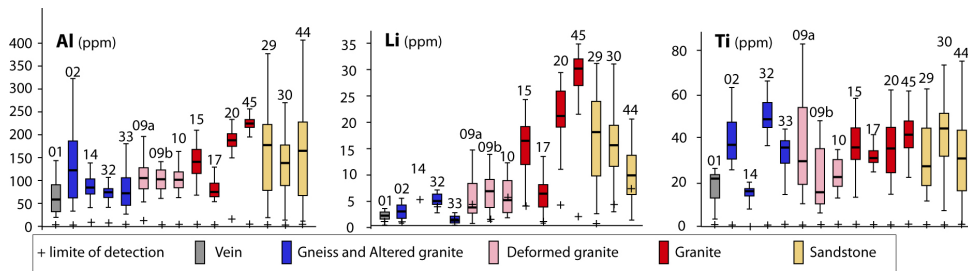
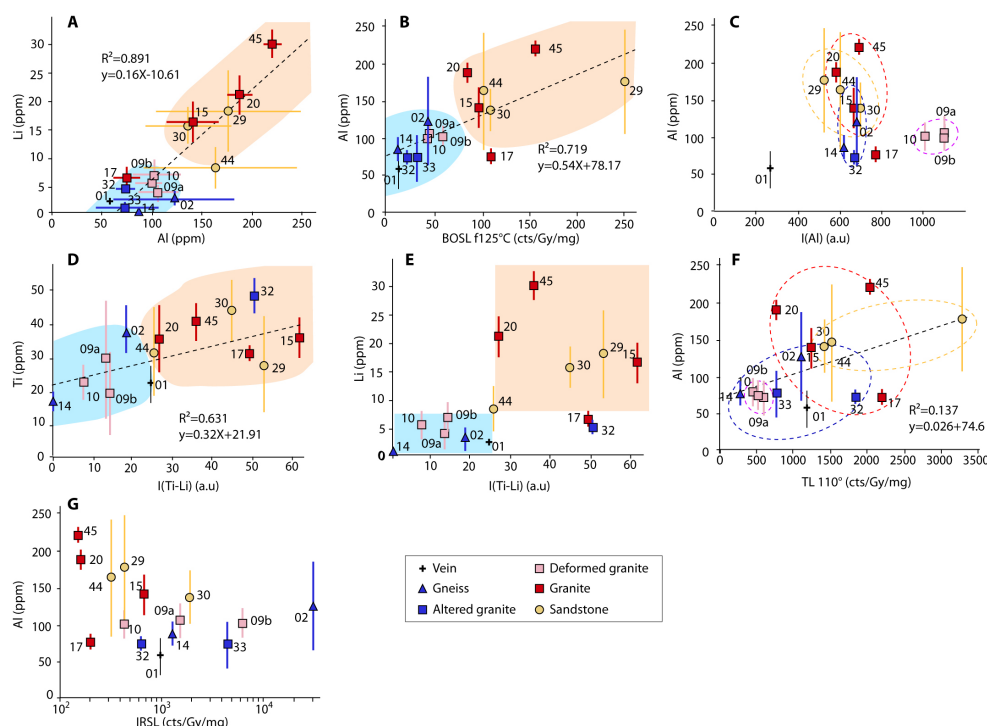


Figure 3: Graphical representations of the Al, Li and Ti contents (ppm) obtained by La-ICPMS on quartz grains extracted from magmatic, metamorphic and sedimentary rocks in the Strengbach basin

Al contents do not discriminate between bedrock types, but median values seem slightly increasing from the quartz vein, gneisses and altered and deformed granites to those of granites. Li contents are scattered with different concentrations related to bedrock types: very low ( $\sim 5$  ppm) in quartz veins/gneisses/altered granites (Turckheim), fairly homogeneous ( $\sim 15$  ppm) in deformed (Bilstein) granites, and high ( $\sim 35$  ppm) but with large scatter in granites (except #17) and sandstones. Ti content does not seem to discriminate between bedrock types. Gneisses and Altered granites showing a wide dispersion between samples from the same rock type whereas Ti content



values for granites and sandstones are less scattered. The ratio between the median Al and Li contents shows a  
 355 strong positive correlation ( $R^2=0.891$ ; Fig.4A), highlighting again two main groups of bedrocks as previously  
 reported with the trapped-charge methods (ESR/OSL)(Figs.2A, 2D and 2G).



**Figure 4: Graphical representations of data obtained by ESR, OSL and La-ICPMS on quartz grains extracted from magmatic, metamorphic and sedimentary rocks in the Strengbach basin. A) Li (ppm) Vs Al (ppm); B) Al (ppm) Vs BOSL<sub>125°C</sub>; C) Al (ppm) vs ESR Al; D) Ti (ppm) vs ESR Ti-Li; E) Li (ppm) vs ESR Ti-Li; F) Al (ppm) vs TL<sub>110°C</sub>; G) Al (ppm) vs IRSL.**

### 5.3 Relation between OSL sensitivities/ESR intensities and Al, Ti, Li concentrations

First, comparison between Al contents and BOSL<sub>f125°C</sub> sensitivities show a good correlation (Fig. 4B,  $R^2=0.719$ ). Again, it highlights the two usual groups: i.e. low sensitivity and low Al content for the quartz vein, gneisses, Turckheim and Bilstein altered granites vs high sensitivity and high Al contents for the remaining granites and sandstones, except for sample #17 showing rather low Al content. Second -and interestingly- no linear correlation is observed between Al contents and ESR Al intensities (Fig.4C). Third -by contrast- Ti contents correlate well with ESR Ti-Li intensities (Fig.4D,  $R^2=0.631$ ), with the same two groups as above except the sample #32 (gneiss) which includes the granite/sandstone group (Fig.4D). Fourth, comparison between Li contents with ESR Ti-Li intensities do not allow the calculation of correlation line but highlight the same dichotomy, with samples #17 and 32 plotting as outliers (Fig.4E) as well as the comparison between Al contents with IRSL sensitivity (Fig.4F)



## 6 Discussion

### 6.1 Quartz OSL sensitivities and ESR intensities in source bedrocks

Quartz aliquots with low OSL sensitivity signals are documented in plutonic or metamorphic bedrocks and the reported values generally fall within the following range between ~10 to 500 counts/Gy or slightly higher values for siliciclastic rocks (Sawakuchi et al., 2011a; Chithambo et al., 2007; Capaldi et al., 2022; Niyonzima, 2020; Mineli et al., 2021; Alexanderson, 2022). Our dataset also exhibits low quartz OSL sensitivities (i.e. ~10 to ~250 cts/Gy/mg or 15 to 615 cts/Gy) which fall into the previous range. We also notice a strong correlation ( $R^2=0.647$ ,  $R^2=0.804$  without #32 outlier, Fig 2B, -) between the  $TL_{110^\circ C}$  peak and the first second of the OSL signal ( $BOSL_{f125^\circ C}$ ) sensitivities, a laboratory observation widely acknowledged in the literature (Murray and Wintle, 2000; Jain et al., 2003; Mineli et al., 2021). The sensitivity present characteristics which seem correlating with the lithologies of source bedrocks, also reported with ESR intensities derived from Ti-Li, Ti-H, OBAT and DAT centres (Fig 2C, D and E). We assume here that (i) sensitivities correspond to the amount of signal growth per unit dose (i.e. expressed as sensitivity =  $\Delta E/\Delta Gy$ , Liu et al 2022) and (ii) the received natural dose is high enough to be considered identical for all samples. We thus propose that the measured ESR intensities obtained on quartz of bedrocks are comparable to their sensitivities. Importantly, our results indicate that ESR and OSL sensitivities may depend on intrinsic properties of the source bedrock, as already pointed out by other studies (Duttine et al, 2003, Lutoev, 2005; Kotova et al., 2007, 2008; Shimada et al., 2013; Sawakuchi et al., 2011a; Capaldi et al. 2022; Niyonzima, 2020). In this respect, quartz extracted from a quartz vein and composite metamorphic bedrocks record the lowest ESR and OSL sensitivities values, as well as plutonic samples collected within a shear zone (i.e. samples #9A and 9B in the Bilstein fault zone). Intermediate ESR and OSL sensitivities values are observed in quartz collected from plutonic rocks and sandstones. So once again, our results thus clearly indicate that (i) inter-sample variability is characteristic of the geological origin, and that (ii) two main groups can be obviously distinguished based on the analysis of different measured signals.

The Ti-Li ESR and  $BOSL_{f125^\circ C}$  sensitivities appear to correlate (Fig 2F) but no correlation was observed between ESR-Al and  $BOSL_{f125^\circ C}$  sensitivities (Fig 2G), which would indicate that different centres may be involved in ESR and OSL signals.

### 6.2 Relation sensitivities of trapped charge methods and trace element composition

The potential relationship between quartz OSL/ESR sensitivities and geological sources in relation to different natures and concentrations of impurities (trace elements) and/or vacancies within the crystal lattice responsible for OSL emission centres and/or traps was preliminary discussed in Preusser et al. (2006). We thus aim to further explore this relationship by specifically looking at the type and the concentration of impurities using trace element contents in our samples. Trace elements are preferentially incorporated into the quartz lattice on substitutional (i.e. Al, Ti, Ge) or interstitial (i.e. Li, Na, K) positions. First, we report a significant linear correlation ( $R^2=0.891$ ) between quartz's Al and Li contents so that two groups of quartz-bearing bedrocks can be distinguished in the Strengbach catchment (Fig. 4A). Interestingly, this relation may be explained if Li is mostly structurally incorporated for compensating Al in the quartz structure. Our data also agree with previous results showing that Li may be exclusively incorporated into the structural channels parallel to the c-axis of the quartz lattice as charge balancing cation for Al in granite and pegmatite (Stavrov et al. 1978; Götze et al., 2004).



#### 410 6.2.1 OSL

A good correlation is observed between Al contents and  $BOSL_{f_{125^{\circ}C}}$  (Fig. 4B  $R^2=0.719$ ), as already reported in Alonso et al. (1983) and Preusser et al. (2009), whereas it is much weaker between Al contents and  $TL_{110^{\circ}C}$  (Fig. 4F  $R^2=0.137$ ) signals. On the one hand, as  $Al^{3+}$  substitutes to  $Si^{4+}$  in the quartz crystalline lattice, increasing Al contents are generally well correlated with the compensating alkali ions (Li+Na+K). On the other hand, Godfrey-Smith and Cada (1996) and Gulnarik et al. (2015) reported IRSL signals resulting from feldspar impurities with  $Al^{3+}$  (Alkali)<sup>+</sup> complex in the quartz lattice itself. OSL data from the Strengbach's quartz-bearing bedrocks do not evidence the second correlation (Fig. 4G), thereby excluding Al enrichment by feldspar impurities. OSL data are instead consistent with Itoh et al.'s (2002) model for which the  $TL_{110^{\circ}C}$  peak intensity is linked to the concentration of alkali-compensated Al centres (also determined by ICP-MS, Vartanian et al., 2000).

#### 420 6.2.2 ESR

First, no correlation is observed when we compare ESR-Al intensities with Al trace contents (Fig. 4C), contrary to what was reported by Usami (2010 in Shimada et al., 2016). However, Götze et al. (2004) obtained similar results as those presented here; the absence of such correlation was assumed to be caused by the fact that not all substitutional Al atoms are present in the form of paramagnetic centres. This phenomenon occurs when the radiation dose is too low to transform trace element defects from the non-paramagnetic precursor state into paramagnetic centres (Götze et al. 2004). Second, if no statistical correlation between ESR-Ti-Li intensities and Li trace contents is observed at first glance, the latter are systematically lower in the gneisses/deformed granites (Bilstein) group than in the granites/sandstones group (Fig. 4E). Note also that the gneiss sample #14 void of Li content (Fig. 3) shows neither Ti-Li intensity nor Ti-H intensity accordingly (Fig. 2D). This potential relation between Li content and Ti-Li ESR intensity was already mentioned by Rink (1993), who reported high electron paramagnetic resonance (EPR) in quartz extracted from Li-rich pegmatite. In the same way, Liu et al. (2022) concluded that ESR sensitivity increase is rather linked to a greater mobility of  $Li^{+}$  and  $H^{+}$  ions than Al with temperature. This high mobility of  $Li^{+}$  and  $H^{+}$  probably leads to Li loss from the quartz lattice in gneisses and deformed Bilstein granites. Although this leakage of Li during modification of the quartz lattice by temperature and/or pressure remains hypothetical at this stage, we argue that this potential significant finding should be further investigated in future studies.

Third, Ti trace content alone does not discriminate source bedrocks (Fig. 3). However, the significant correlation ( $R^2=0.631$ ) between ESR-Ti-Li intensity and Ti contents (Fig. 4D) allows distinguishing, anew, the two usual groups of source bedrock. The increasing amount of Ti content may cause a general increase of the Ti-Li ESR signal, and an increase of substitution of Si by Ti. The non-zero intercept of our data on the Ti axis (Fig. 4D) may also suggest the occurrence of inherited non-structurally incorporated Ti (Götze et al., 2004). It may also be related to a lack of Li compensator (see for instance #14 in Fig.4E) and this should be further investigated.

### 6.3 Relation between ESR/OSL sensitivity and conditions of crystallization and deformation

445 Because we assume that Al and Ti ESR centres from all treated samples have reached saturation as crystallisation/diagenesis of all quartz-bearing bedrocks took place >200 millions of years ago, we can compare measured ESR intensities with OSL sensitivities. One generally acknowledges that the large variability reported



in bedrock OSL sensitivities is linked to temperature and pressure conditions during metamorphism or magmatic crystallization (e.g. Sawakuchi et al., 2011b): quartz with low OSL sensitivity signals were detected in plutonic or metamorphic bedrocks that have experienced high temperature and pressure conditions (Lukas et al., 2007; Jeong and Choi, 2012; Zular et al., 2015; Guralnik et al., 2015). Variability in ESR sensitivities for different bedrock types was likewise pointed out in different settings: Duttine et al. (2003) (Al, Ti-Li, Ti-H intensities); Kotova et al., (2008) (Al intensities); Shimada et al., 2013 (Al and Ti-Li intensities).

In this respect, two outcomes of this study well match previous observations. First, our observations in general agree with Kotova et al (2008)'s suggestion: lower number ESR-Al and ESR-Ge defects (i.e. Ge and Ti defects being similarly ion compensated defects) are caused either by quartz vein crystallization from highly oversaturated silicium solutions or from solutions with low contents of Al or Ge, possibly reflecting the initial fluid composition.. Second, similarly to Duttine et al. (2003), our quartz vein sample (#1) displays both (i) low ESR and OSL sensitivities and (ii) low Al and Li trace contents (Fig. 3, 4A, 4B, 4C).

### 6.3.1 Effect of temperature

Higher crystallization temperature may increase the concentration of Si- and O-vacancies (Preusser et al., 2009) and also favour the substitution of  $\text{Si}^{4+}$  by  $\text{Al}^{3+}$  and  $\text{Ti}^{4+}$  ions, which produce the defects underpinning luminescence in quartz (Dennen et al., 1970; Götze et al., 2001; Wark and Watson, 2006).  $\text{Ti}^{4+}$  can substitute to  $\text{Si}^{4+}$  but only at high temperature, resulting in exsolution during cooling (Götze et al., 2004), while  $[\text{TiO}_4/\text{Li}^+]^0$  and  $[\text{TiO}_4/\text{H}^+]^0$  populations are significantly increased by heating (Poolton, 2000). Also, sensitivity change to irradiation is contrasted between Al/Ti-Li centres (i.e. steady increase with heating) and Ti-H (i.e. increase up to  $\sim 500^\circ\text{C}$  and decrease  $> 500^\circ\text{C}$ ; Liu et al (2022)). However, Schilles et al. (2001) observed an increase in both Ti-H and Ti-Li intensities up to  $700^\circ\text{C}$  before the former reduce and the latter stabilise at higher temperatures.

Importantly, not only are these observations somehow inconsistent with each other (e.g. contrasting behaviour, different threshold temperatures...), but they also only partly fit our data. On the one hand, the formation temperature of all sampled metamorphic and plutonic bedrocks ranges between  $350^\circ\text{C}$  and  $660^\circ\text{C}$  (Table 1). This falls into the aforementioned temperature ranges for which changes in intrinsic OSL and ESR sensitivity characteristics were reported. In particular, all sampled gneisses underwent the highest temperatures ( $600$ - $660^\circ\text{C}$ ; Table 1) during their metamorphic event(s). If one would have expected the highest increase in Ti-Li and Ti-H ESR sensitivities for these metamorphic rocks, we observe the contrary as granitic bedrocks (i.e. samples #15,17,20,45; the “undeformed” granites) have higher ESR sensitivities than the gneissic samples (Fig. 2E). On the other hand, Al intensities do not display the same pattern ( Fig. 2F, 2G), suggesting that they behave differently, and this observation agrees with those of Fukushi (1989), Poolton (2000), Schilles et al. (2001), who demonstrated that heating does not alter the sensitivity of the Al centre in quartz. Also, low OSL sensitivities are not only observed for the gneisses but also in granitic bedrock which undergone deformation (Bilstein Fault zone for samples #9A, 9B, 10). This agrees with previous observations (Sawakuchi et al., 2011b, 2020; Gulnarik et al., 2015), suggesting that heating do not favour OSL sensitisation and may therefore reset the sensitivity.

As the initial (i.e. pre-heating/pre-deformation) OSL and ESR characteristics of the metamorphic and deformed bedrocks in the Strengbach catchment are unknown, whether the measured sensitivities have been modified -or not- over time remains an open question. However, both metamorphic rocks are paragneisses (Table 1) and are thereby meta-sediments containing recycled quartz grains (i.e. somehow similar to the sandstone bedrocks). One





can thus expect that the sensitivity of these bedrocks was higher prior to metamorphism or deformation (sediment sensitivity e.g. [Pietsch et al. 2008](#)). Finally, note that samples #15,17,20,45 (i.e. undeformed granites) present the highest ESR and OSL signal sensitivities as well as the highest Al, Ti and Li trace contents but were not affected by metamorphism nor by tectonic deformation.

### 6.3.2 Effect of pressure

Pressure is the other parameter that could explain luminescence variations and sensitivities in the investigated bedrocks. In this respect, all samples that underwent high pressure during metamorphism (4-7 kbar; Table 1) along with those located in the tectonic shear zone (Fig. 1) show both lowest OSL and ESR intensities. This suggests that pressure can be one of the prevailing factors driving changes in OSL/ESR sensitivities. If decrease of OSL sensitivities and signal resetting within a fault zone was already reported ([Odlum et al., 2022](#); [Hu et al., 2024](#)), the effect of pressure during metamorphism is still poorly understood. As for ESR sensitivity, if pressure does not seem to be a prevailing factor concerning the ESR-Al centre ([Fukushi, 1989](#)), no information is found concerning its role on the sensitivity of the Ti-Li and Ti-H centres.

### 6.3.3 Combined effects

We notice that heat and pressure, contrary to their effect on Ti-Li and Ti-H centres, do not substantially modify the paramagnetic capacity of the Al centres in quartz. This observation probably also applies to quartz veins: whereas ESR-Al intensities in hyaline quartz from vein do not differ from those of the bedrock, ESR-Ti centres do ([Duttine et al., 2003](#)). In conclusion, ESR-Al intensities are less discriminant than ESR-Ti intensities between different quartz rocks and sources, unless the photosensitivity of the ESR-Al centre is also considered (Fig. 2C). In this case, this could suggest that the ESR-Al intensities are more related to the initial conditions of mineral formation in relation to the fluid composition (see section 5.3).

### 6.4 Quartz sensitisation in recycled and mature sediments

[Pietsch et al. \(2008\)](#) showed that mature and recycled quartz presents higher OSL sensitivity values than parent bedrocks, which suggests that surficial transport processes produce sensitisation in quartz grains. In this respect, we can assume that the sandy sediments that later formed the Triassic sandstones in the Strengbach catchment are sensitive due to previous sedimentary cycles. Indeed, the sediments that make up the sandstones were deposited in a fluvial context ([Bofill et al., 2024](#)), and therefore underwent one or more cycles of remediation by exposure to light and natural irradiation when they were buried. Whilst the highest OSL sensitivity found in the sandstone sample #29 seems matching this assumption (Fig. 2A), the two other sandstone samples (#30 and 44) present similar OSL sensitivities than those of the granites.

The sensitisation of ESR centres with optical bleaching-irradiation cycles is currently unknown. Our data show that none of the sandstone samples have higher ESR-Al sensitivities than granite and gneiss samples (Fig. 2G). The Ti-Li and Ti-H centres show ESR sensitivities for sandstones that are in the higher value of our dataset, but that remain within the range of undeformed granites. In fact, the latter are mostly indistinguishable from sandstones except for their bleaching rate (Fig. 2C).



## 7 Conclusions

This study provides valuable insights into the OSL and ESR sensitivities of quartz extracted from diverse geological settings. Our findings demonstrate that these sensitivities are strongly influenced by the intrinsic properties of the source bedrock, including its lithology, crystallization conditions, and deformation history.

A significant relationship between source rock characteristics and (palaeo)dosimetric intensities for both Optically Stimulated Luminescence (OSL) and Electron Spin Resonance (ESR) was identified, particularly for Ti centres in ESR. Quartz from deformed plutonic and from metamorphic bedrocks consistently shows low OSL sensitivity and ESR Ti-centres intensities, while intermediate sensitivity and intensities values are observed in quartz from plutonic rocks and sandstones.

The trace element composition appears to influence the ESR and OSL sensitivities of quartz. Furthermore, geological processes such as recrystallization, metamorphism, and anatexis significantly affect ESR Ti-Li and Ti-H centre intensities as well as BOSL<sub>f125°C</sub> signals, especially, the pressure could be one of the prevailing factors driving changes in OSL/ESR sensitivities. Conversely, ESR-Al centre intensities appear to be governed by the initial fluid composition and crystallization environment. Enhanced OSL sensitivity in mature and recycled sediments (sandstones) highlights the influence of sedimentary transport and reworking on OSL sensitivity but have to be investigated for ESR.

These insights have significant implications for geochronology and sediment provenance analysis, where precise interpretations of luminescence and ESR signals are essential. More specifically, caution is advised when dating sediment provided by metamorphic terrains, due to the potential absence or weakness of ESR Ti-Li and Ti-H signals, which can pose challenges for reliable ESR analysis.

Finally, future studies should investigate whether these patterns are consistent across different geological catchments and explore their manifestation in sediments derived from these source rocks. Future research should explore whether these findings are consistent across different catchments and if these signatures are present in sediments draining these source rocks. Additionally, the significance of hydrogen content, undetectable by ICP and currently being determined by other means, warrants further investigation.

## Acknowledgement

The authors acknowledge the ANR – FRANCE (French National Research Agency) for its financial support of the QUARTZ project N° ANR-21-CE01-0014. The ESR spectrometer of the Muséum nationale d'Histoire naturelle, France was bought with the financial support of the 'DIM MAP Île-de-France' program. The authors would like to thank Catherine Lerouge (BRGM) for her scientific expertise in trace element analysis and for the fruitful discussions.

## Author contribution

H. Tissoux, Magali Rizza, P. Voinchet and C. Aupart designed the experiments. All the authors performed field work and sampling. M. Boulay made the samples physical and chemical preparation. Geological setting was established by G. Rixhon and C. Aupart. P. Voinchet carried out ESR measurements. M Rizza carried out OSL measurements C. Aupart carried out LA-ICPMS measurements. P. Voinchet and H. Tissoux analysed the ESR data. Magali Rizza, P. Valla and G. Rixhon analysed the OSL data. C. Aupart and P. Lach analysed the LA-ICPMS data. H. Tissoux and P Voinchet prepared the manuscript with contributions from all co-authors.



## Competing interests

The authors declare that they have no conflict of interest.

## References

- Alexanderson, H., 2022. Luminescence characteristics of Scandinavian quartz, their connection to bedrock provenance and influence on dating results. *Quaternary Geochronology* 69, 101272. <https://doi.org/10.1016/j.quageo.2022.101272>
- Allen, P.A., 2017. Sediment Routing Systems: The Fate of Sediment from Source to Sink [WWW Document]. Cambridge Core. <https://doi.org/10.1017/9781316135754>
- Alonso P. J., Halliburton L. E., Kohnke E. E., and Bossoli R. B. (1983) X-ray induced luminescence in crystalline SiO<sub>2</sub>. *J. Appl. Phys.* 54,5369–5375.
- Amiotte-Suchet, P., Aubert, D., Probst, J.L., Gauthier-Lafaye, F., Probst, A., Andreux, F., & Viville, D., 1999.  $\delta^{13}\text{C}$  pattern of dissolved inorganic carbon in a small granitic catchment: the Strengbach case study (Vosges mountains, France). *Chemical Geology*, 159:129-145. [https://doi.org/10.1016/S0009-2541\(99\)00037-6](https://doi.org/10.1016/S0009-2541(99)00037-6)
- Beerten, K., Stesmans, A., 2006a. Some properties of Ti-related paramagnetic centres relevant for electron spin resonance dating of single sedimentary quartz grains. *Applied Radiation and Isotopes* 64, 594-602. <https://doi.org/10.1016/j.apradiso.2005.12.001>
- Beerten, K., Stesmans, A., 2006b. The use of Ti centers for estimating burial doses of single quartz grains: A case study from an aeolian deposit Ma old. *Radiation Measurements* 41, 418–424. <https://doi.org/10.1016/j.radmeas.2005.10.004>
- Bofill, L., Bozetti, G., Schäfer, G., Ghienne, J.-F., Schuster, M., Scherer, C., De Souza, E., 2024. Quantitative facies analysis of a fluvio-aeolian system: Lower Triassic Buntsandstein Group, eastern France. *Sedimentary Geology* 465, 106634. <https://doi.org/10.1016/j.sedgeo.2024.106634>
- Bonhomme, M., 1967. Ages radiométriques de quelques granites de Vosges moyennes. *Bull. Serv. Carte géol. Als. Lorr.*, 20(1): 101-106.
- Bøtter-Jensen, L., Agersnap Larsen, N., Mejdahl, V., Poolton, N.R.J., Morris, M.F., McKeever, S.W.S., 1995. Luminescence sensitivity changes in quartz as a result of annealing. *Radiation Measurements* 24 (4), 535-541.
- Capaldi, T.N., Rittenour, T.M., Nelson, M.S., 2022. Downstream changes in quartz OSL sensitivity in modern river sand reflects sediment source variability: Case studies from Rocky Mountain and Andean rivers. *Quaternary Geochronology* 71, 101317. <https://doi.org/10.1016/j.quageo.2022.101317>.
- Chabaux, F., Viville, D., Lucas, Y., Ackerer, J., Ranchoux, C., Bosia, C., Pierret, M.-C., Labasque, T., Aquilina, L., Wyns, R., Lerouge, C., Dezaye, C., & Négrel, P., 2017. Geochemical tracing and modeling of surface and deep water-rock interactions in elementary granitic watersheds (Strengbach and Ringelbach CZOs, France). *Atca Geochimica*, 36:363-366. <https://doi.org/10.1007/s11631-017-0163-5>
- Chithambo, M.L., Preusser, F., Ramseyer, K., Ogundare, F.O., 2007. Time-resolved luminescence of low sensitivity quartz from crystalline rocks. *Radiat. Meas.* 42, 205–212.
- David, M., Sunta, C.M., 1981. Thermoluminescence of quartz e part VIII: estimation of firing temperature in ancient pottery samples. *Indian Journal of Pure & Applied Physics* 19, 1054-1056.
- del Río, I., Sawakuchi, A.O., G'oes, A.M., Hollanda, M.H., Furukawa, N.Y., Porat, N., Negri, F.A., 2021. Luminescence signals of quartz and feldspar as new methods for stratigraphic discrimination and provenance



- analysis of siliciclastic successions: the case of the Parnaíba Basin (Brazil) of West Gondwana. *Basin Res.* 1–22.  
<https://doi.org/10.1111/bre.12590>
- Delmas, M., Calvet, M., Gunnell, Y., Voinchet, P., Manel, C., Braucher, R., Tissoux, H., Bahain, J.-J., Perrenoud,  
 605 C., Saos, T., 2018. Terrestrial  $^{10}\text{Be}$  and electron spin resonance dating of fluvial terraces quantifies quaternary  
 tectonic uplift gradients in the eastern Pyrenees. *Quaternary Science Reviews* 193, 188–211.  
<https://doi.org/10.1016/j.quascirev.2018.06.001>
- Dennen, W.H., Blackburn, W.H., Quesada, A., 1970. Aluminum in quartz as a geothermometer. *Contributions to  
 Mineralogy and Petrology* 27, 332–342. Corpus ID: 119075235
- 610 Duttine, M., Villeneuve, G., Bechtel, F., Demazeau, G., 2002. Caractérisation par résonance paramagnétique  
 électronique (RPE) de quartz naturels issus de différentes sources. *Comptes Rendus Geoscience* 334, 949–955.  
[https://doi.org/10.1016/S1631-0713\(02\)01845-X](https://doi.org/10.1016/S1631-0713(02)01845-X)
- Chithambo, M.L., Preusser, F., Ramseyer, K., Ogundare, F.O., 2007. Time-resolved luminescence of low  
 sensitivity quartz from crystalline rocks. *Radiat. Meas.* 42, 205–212.  
 615 <https://doi.org/10.1016/j.radmeas.2006.07.005>
- Fitzsimmons, K.E., Perić, Z., Nowatzki, M., Lindauer, S., Vinnepand, M., Prud'homme, C., Dave, A.K., Vött, A.,  
 Fischer, P. (2022). Luminescence Sensitivity of Rhine Valley Loess: Indicators of Source Variability?. *Quaternary*,  
 5, 1. <https://doi.org/10.3390/quat5010001>
- Fluck, P., Piqué, A., Schneider, J.-L., Whitechurch, H., 1991. Le socle vosgien / The vosgian basement. *sgeol* 44,  
 620 207–235. <https://doi.org/10.3406/sgeol.1991.1867>
- Wild, B., Daval, D., Beaulieu, E., Pierret, M.-C., Viville, D., Imfeld, G., 2019. In-situ dissolution rates of silicate  
 minerals and associated bacterial communities in the critical zone (Strengbach catchment, France). *Geochimica et  
 Cosmochimica Acta* 249, 95–120. <https://doi.org/10.1016/j.gca.2019.01.003>
- Gall J.C., 2006. Fluvial depositional environment evolving into deltaic setting with marine influences in the  
 625 Buntsandstein of Northern Vosges (France). *Lecture Notes in Earth Sciences* 4, 449–477.  
<https://doi.org/10.1007/BFb0010532>
- Gangloff, S., Stille, P., Pierret, M.-C., Weber, T., & Chabaux, F., 2014. Characterization and evolution of dissolved  
 organic matter in acidic forest soil and its impact on the mobility of major and trace elements (case of the  
 Strengbach watershed). *Geochimica et Cosmochimica Acta*, 130:21–41. <https://doi.org/10.1016/j.gca.2013.12.033>
- 630 Gliganic, L.A., Cohen, T.J., Meyer, M., Molenaar, A., 2017. Variations in luminescence properties of quartz and  
 feldspar from modern fluvial sediments in three rivers. *Quaternary Geochronology* 41, 70–82.  
<https://doi.org/10.1016/j.quageo.2017.06.005>
- Godfrey-Smith D.I., Cada M, 1996; IR Stimulation Spectroscopy of Plagioclase and Potassium Feldspars, and  
 Quartz. *Radiation Protection Dosimetry*, Volume 66, Issue 1–4, 379–385,  
 635 <https://doi.org/10.1093/oxfordjournals.rpd.a031759>
- Götze, J., Plötze, M., Tichomirowa, M., Fuchs, H., Pilot, J., 2001. Aluminum in quartz, as an indicator of the  
 temperature of formation of agate. *Mineralogical Magazine* 65 (3), 407–413.  
<https://doi.org/10.1180/002646101300119484>
- Götze, J., Plötze, M., Graupner, T., Hallbauer, D.K., Bray, C.J., 2004. Trace element incorporation into quartz: A  
 640 combined study by ICP-MS, electron spin resonance, cathodoluminescence, capillary ion analysis, and gas  
 chromatography. *Geochim. Cosmochim. Acta* 68, 3741–3759. <https://doi.org/10.1016/j.gca.2004.01.003>



- Gray, H. J., Jain, M., Sawakuchi, A. O., Mahan, S. A., & Tucker, G. E., 2019. Luminescence as a sediment tracer and provenance tool. *Reviews of Geophysics*, 57. <https://doi.org/10.1029/2019RG000646>
- Guralnik, B., Jain, M., Herman, F., Ankjærgaard, C., Murray, A.S., Valla, P.G., Preusser, F., King, G.E., Chen, R., Lowick, S.E., Kook, M., Rhodes, E.J., 2015. OSL-thermochronometry of feldspar from the KTB borehole, Germany. *Earth and Planetary Science Letters* 423, 232–243. <https://doi.org/10.1016/j.epsl.2015.04.032>
- Hu, G., Zeng-Liu, J., Shao, Y., Qin, K., Gao, Y., 2024. The applications of optically stimulated luminescence dating in active fault and paleo-earthquake studies: A review. *Quaternary International*. 688, 53-62. <https://doi.org/10.1016/j.quaint.2024.01.016>
- Ikeya, M., 1993. *New Applications of Electron Spin Resonance, Dating, Dosimetry, and Microscopy*. World Scientific, Singapore. 520p. <https://doi.org/10.1142/1854>
- Ingicco, T., Van Den Bergh, G.D., Jago-on, C., Bahain, J.-J., Chacón, M.G., Amano, N., Forestier, H., King, C., Manalo, K., Nomade, S., Pereira, A., Reyes, M.C., Sémah, A.-M., Shao, Q., Voinchet, P., Falguères, C., Albers, P.C.H., Lising, M., Lyras, G., Yurnaldi, D., Rochette, P., Bautista, A., De Vos, J., 2018. Earliest known hominin activity in the Philippines by 709 thousand years ago. *Nature* 557, 233–237. <https://doi.org/10.1038/s41586-018-0072-8>
- Itoh, N., Stoneham, D., Stoneham, A.M., 2002. Ionic and electronic processes in quartz: Mechanisms of thermoluminescence and optically stimulated luminescence. *Journal of Applied Physics*. Volume 92, Issue 9, 1, 5036-5044. <https://doi.org/10.1063/1.1510951> - Corpus ID: 123022799
- Jain, M., Murray, A.S., Bøtter-Jensen, L., 2003. Characterisation of blue-light stimulated luminescence components in different quartz samples: implications for dose measurement. *Radiat. Meas.* 37, 441–449. [https://doi.org/10.1016/S1350-4487\(03\)00052-0](https://doi.org/10.1016/S1350-4487(03)00052-0).
- Jani, M.G., Bossoli, R.B., Halliburton, L.E., 1983. Further characterization of the E'1 center in crystalline SiO<sub>2</sub>. *Phys. Rev. B* 27, 2285-2293. <https://doi.org/10.1103/PhysRevB.27.2285>
- Jeong, G.Y., Choi, J.-H., 2012. Variations in quartz OSL components with lithology, weathering and transportation, *Quaternary Geochronology*, doi: 10.1016/j.quageo.2012.02.023
- Kotova et al., 2007 Paramagnetic centers in quartz of basic industry deposits. *Acta Crystallographica Section A: Foundations and Advances*. 249-s249. <https://doi.org/10.1107/S0108767307094378>
- Kotova, E.N., Lyutov, V.P., Kuznetsov, S.K., 2008. Aluminum and germanium paramagnetic centers in vein quartz and rock crystals from the Subpolar Urals. *Geol. Ore Deposits* 50, 634-641. <https://doi.org/10.1134/S1075701508070155>
- Koul, D.K., Chougankar, M.P., 2007. The pre-dose phenomenon in the OSL signal of quartz. *Radiation Measurements* 42, 1265-1272. <https://doi.org/10.1016/j.radmeas.2007.04.001>
- Koul, D.K., 2006. Role of alkali ions in limiting the capacity of the 110 °C peak of quartz to remember the firing temperature. *Applied Radiation and Isotopes* 64, 110-115. <https://doi.org/10.1016/j.apradiso.2005.07.008>
- Kratinova, Z., Schulmann, K., Edel, J.B., Ježek, J., Schaltegger, U., 2007. Model of successive granite sheet emplacement in transtensional setting: integrated microstructural and anisotropy of magnetic susceptibility study. *Tectonics* 26 (6), 1–7. , doi:10.1029/2006TC002035
- Latouche, L., Fabriès, J., Guiraud, M., 1992. Retrograde evolution in the Central Vosges mountains (northeastern France): implications for the metamorphic history of high-grade rocks during the Variscan orogeny. *Tectonophysics* 205, 387–407. [https://doi.org/10.1016/0040-1951\(92\)90444-B](https://doi.org/10.1016/0040-1951(92)90444-B)



- Li, S.H., 2002. Luminescence sensitivity changes of quartz by bleaching, annealing and UV exposure. *Radiation Effects and Defects in Solids* 157, 357-364. <https://doi.org/10.1080/10420150212998>
- Liu, C.-R., Ji, H., Li, W.-P., Wei, C.-Y., Yin, G.-M., 2022. The relationship between irradiation sensitivity of quartz Al and Ti centers and baking temperature by volcanic lava flow: Example of Datong volcanic group, China. *Radiation Measurements* 157, 106823. <https://doi.org/10.1016/j.radmeas.2022.106823>
- Lukas, S., Spencer, J.Q.G., Robinson, R.A.J., Benn, D.I., 2007. Problems associated with luminescence dating of Late Quaternary glacial sediments in the NW Scottish Highlands. *Quaternary Geochronology* 2, 243–248. <https://doi.org/10.1016/j.quageo.2006.04.007>
- Lutoev, V. P., 2005. Application of the ESR method in geological correlation problems. *Applied Magnetic Resonance* 28, 311-330. <https://doi.org/10.1007/BF03166764>
- McKeever, S.W.S., Bøtter-Jensen, L., Agersnap Larsen, N., Mejdah, V., Poolton, N.R.J., 1996. Optically stimulated luminescence sensitivity changes in quartz due to repeated use in single aliquot readout: experiments and computer simulations. *Radiation Protection Dosimetry* 65 (1-4), 49-54. <https://doi.org/10.1093/oxfordjournals.rpd.a031680>
- Mineli, T.D., Sawakuchi, A.O., Guralnik, B., Lambert, R., Jain, M., Pupim, F.N., Rio, I. del, Guedes, C.C.F., Nogueira, L., 2021. Variation of luminescence sensitivity, characteristic dose and trap parameters of quartz from rocks and sediments. *Radiation Measurements* 144, 106583. <https://doi.org/10.1016/j.radmeas.2021.106583>
- Moska, P., Murray, A.S., 2006. Stability of the quartz fast-component in insensitive samples. *Radiation Measurements* 41, 878-885. <https://doi.org/10.1016/j.radmeas.2006.06.005>
- Murray, A.S., Roberts, R.G., 1998. Measurement of the equivalent dose in quartz using a regenerative-dose single-aliquot protocol. *Radiation Measurements* 29, 503-515. [https://doi.org/10.1016/S1350-4487\(98\)00044-4](https://doi.org/10.1016/S1350-4487(98)00044-4)
- Murray, A., Wintle, A.G., 2000. Luminescence dating of quartz using an improved single-aliquot regenerative-dose protocol. *Radiation Measurements* 32, 57-73. [https://doi.org/10.1016/S1350-4487\(99\)00253-X](https://doi.org/10.1016/S1350-4487(99)00253-X)
- Nelson, M.S., Eppes, M.C., Rittenour, T.M., 2022. Quartz luminescence sensitivity from sediment versus bedrock in highly weathered soils of the Piedmont of North Carolina, south-eastern USA: *Quaternary Geochronology*, p. 101343. <https://doi.org/10.1016/j.quageo.2022.101343>.
- Niyonzima, P., Sawakuchi, A.O., Jain, M., Kumar, R., Minelli, T.D., del Río, I., Pupim, F.N., 2020. Radiofluorescence of quartz from rocks and sediments and its correlation with thermoluminescence and optically stimulated luminescence sensitivities. *Ancient TL* 38(1),11-20. <https://doi.org/10.1016/j.epl.2018.04.006>
- Odlum, M. L., Rittenour, T., Ault, A. K., Nelson, M., Ramos, E. J., 2022. Investigation of quartz luminescence properties in bedrock faults: Fault slip processes reduce trap depths, lifetimes, and sensitivity. *Radiation Measurements*, 155, 106784. <https://doi.org/10.1016/j.radmeas.2022.106784> Corpus ID: 248765973
- Ono, Y., Naruse, T., Ikeya, M., Kohno, H., Toyoda, S., 1998. Origin and derived courses of eolian dust quartz deposited during marine isotope stage 2 in East Asia, suggested by ESR signal intensity. *Global and Planetary Change* 18, 129-135. [https://doi.org/10.1016/S0921-8181\(98\)00012-5](https://doi.org/10.1016/S0921-8181(98)00012-5)
- Owen M. Williams, Barnaby W. Smith, Nigel A. Spooner, 2022. A role for oxygen vacancies in quartz luminescence, *Radiation Measurements*, Volume 154, 106774. <https://doi.org/10.1016/j.radmeas.2022.106774>
- Pearce, N.J.G., Perkins, W.T., Westgate, J.A., Gorton, M.P., Jackson, S.E., Neal, C.R., Chenery, S.P., 1997. A Compilation of New and Published Major and Trace Element Data for NIST SRM 610 and NIST SRM 612 Glass Reference Materials. *Geostandards Newsletter* 21, 115–144. <https://doi.org/10.1111/j.1751-908X.1997.tb00538.x>



- Pietsch, T.J., Olley, J.M., Nanson, G.C., 2008. Fluvial transport as a natural luminescence sensitiser of quartz. *Quaternary Geochronology* 3, 365-376. <https://doi.org/10.1016/j.quageo.2007.12.005>
- 725 Polymeris, G.S., Sakalisa, A., Papadopoulou, D., Dallas, G., Kitis, G., Tsirliganis, N.C., 2007. Firing temperature of pottery using TL and OSL techniques. *Nuclear Instruments and Methods in Physics Research A* 580, 747-750. <https://doi.org/10.1016/j.nima.2007.05.139>
- Poolton, N.R.J., Smith, G.M., Riedi, P.C., Bulur, E., Bøtter-Jensen, L., Murray, A.S., Adrian, M., 2000. Luminescence sensitivity changes in natural quartz induced by high temperature annealing: a high frequency EPR and OSL study. *Journal of Physics D: Applied Physics* 33, 1007-1017. <https://doi.org/10.1088/0022-3727/33/8/318>
- 730 Preusser et al., 2009 – Earth science review Pearce, N.J.G., Perkins, W.T., Westgate, J.A., Gorton, M.P., Jackson, S.E., Neal, C.R., & Chenery, S.P., 1997. A Compilation of New and Published Major and Trace Element Data for NIST SRM 610 and NIST SRM 612 Glass Reference Materials. *Geostandards Newsletter*, 21(1):115-144. <https://doi.org/10.1111/j.1751-908X.1997.tb00538.x>
- 735 Preusser, F., Ramseyer, K., Schlüchter, C., 2006. Characterization of low OSL intensity quartz from the New Zealand Alps. *Radiation Measurements* 41, 871-877.
- Rey, P., Burg, J.-P., Caron, J.-M., 1992. Middle and Late Carboniferous extension In the Variscan Belt: structural and petrological evidences from the Vosges massif (Eastern France). *Geodinamica Acta* 5, 17–36. <https://doi.org/10.1080/09853111.1992.11105217>
- 740 Rhodes, E.J., Pownall, L., 1994. Zeroing of the OSL signal in quartz from young glaciofluvial sediments. *Radiat. Meas.* 23, 329-333
- Rink, W.J., Rendell, H., Marseglia, E.A., Luff, B.J., Townsend, P.D., 1993. Thermoluminescence spectra of igneous quartz and hydrothermal vein quartz. *Phys Chem Minerals* 20. <https://doi.org/10.1007/BF00215106>
- Rink, W.J., Rhodes, E.J., Grün, R., 1994. Thermoluminescence from igneous and natural hydrothermal vein quartz: dose response after optical bleaching. *Radiat. Meas.* 23, 159–173.
- 745 Rixhon, G., Briant, R.M., Cordier, S., Duval, M., Jones, A., Scholz, D., 2017. Revealing the pace of river landscape evolution during the Quaternary: recent developments in numerical dating methods. *Quaternary Science Reviews* 166, 91-113. <https://doi.org/10.1016/j.quascirev.2016.08.016>
- Sawakuchi, A.O.; Blair, M.W.; De Witt, R.; Faleiros, F.M.; Hyppolito, T.; Guedes, C.C.F., 2011a. Thermal history versus sedimentary history: OSL sensitivity of quartz grains extracted from rocks and sediments. *Quat. Geochronol.* 6, 261–272.
- 750 Sawakuchi AO, DeWitt R, Faleiros FM., 2011b. Correlation between thermoluminescence sensitivity and crystallization temperatures of quartz: potential application in geothermometry. *Radiation Measurements* 46: 51–58. <https://doi.org/10.1016/j.radmeas.2010.08.005>.
- 755 Sawakuchi AO, Rodrigues FCG, Mineli TD, Mendes VR, Melo DB, Chiessi CM, Giannini PCF., 2020. Optically Stimulated Luminescence Sensitivity of Quartz for Provenance Analysis. *Methods Protoc.* Jan 13;3(1):6. <https://doi.org/10.3390/mps3010006>. PMID: 31941007; PMCID: PMC7189674.
- Sawakuchi, A.O., Jain, M., Mineli, T.D., Nogueira, L., Bertassoli, D.J., Jr., Häggi, C., Sawakuchi, H.O., Pupim, F.N., Grohmann, C.H., Chiessi, C.M., et al., 2018. Luminescence of quartz and feldspar fingerprints provenance and correlates with the source area denudation in the Amazon River basin. *Earth Planet. Sci. Lett.*, 492, 152–162.
- 760





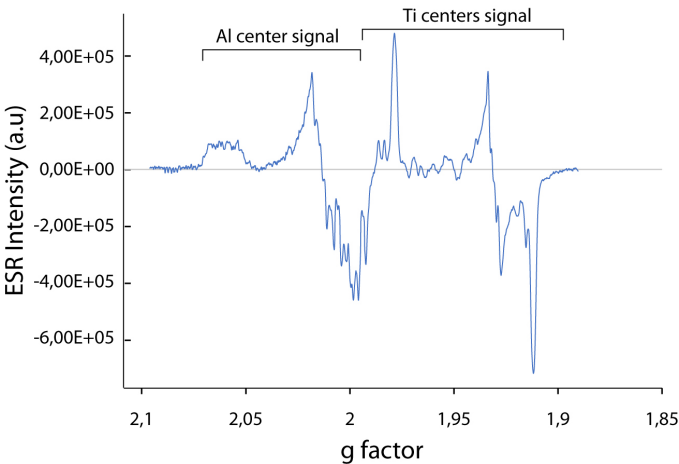
- Schilles, T., Poolton, N.R.J., Bulur, E., Bøtter-Jensen, L., Murray, A.S., Smith, G.M., Riedi, P.C., Wagner, G.A., 2021. A multi-spectroscopic study of luminescence sensitivity changes in natural quartz induced by high-temperature annealing. *Journal of Physics D: Applied Physics*, Volume 34, Issue 5, 7, 722-731.
- Schulmann, K., 2002. Rapid burial and exhumation during orogeny: Thickening and synconvergent exhumation of thermally weakened and thinned crust (Variscan orogen in Western Europe). *American Journal of Science* 302, 856–879. <https://doi.org/10.2475/ajs.302.10.856>
- Schulmann, K., Martinez Catalan, J.R., Lardeaux, J.M., Janoušek, V., Oggiano, G., 2014. The Variscan orogeny: extent, timescale and the formation of the European crust. *Geol. Soc. Lond. Spec. Publ.* 405, 1–6.
- Shimada, A., Takada, M., Toyoda, S., 2013. Characteristics of ESR signals and TLCLs of quartz included in various source rocks and sediments in Japan: A clue to sediment provenance. *Geochronometria* 40, 334-340. <https://doi.org/10.2478/s13386-013-0111-z>
- Shimada, A., Takada, M., Toyoda, S., 2016. Electron spin resonance signals of quartz in present-day river bed sediments and possible source rocks in the Kizu River basin, Western Japan. *Geochronometria* 43, 155-161. <https://doi.org/10.1515/geochr-2015-0039>
- Skrzypek, E., Stipska, P., & Cocherie, A., 2012. The Origin of zircon and the significance of U-Pb ages in high-grade metamorphic rocks: a case study from the Variscan orogenic root (Vosges Mountains, NE France). *Contrib. Mineral Petrol.*, 164:935-957. <https://doi.org/10.1007/s00410-012-0781-1>
- Skrzypek, E., Schulmann, K., Tabaud, A.S., Edel, J.B., 2014. Palaeozoic evolution of the Variscan Vosges Mountains. *Geol. Soc. Lond. Spec. Publ.* 405, 45–75.
- Souza, P.E., Pupim, F.N., Mazoca, C.E.M., Rio, I.D., Mineli, T.D., Rodrigues, F.C.G., Porat, N., Hartmann, G.A., Sawakuchi, A.O., 2023. Quartz OSL sensitivity from dating data for provenance analysis of pleistocene and holocene fluvial sediments from lowland Amazonia. *Quaternary Geochronology* 74, 101422. <https://doi.org/10.1016/j.quageo.2023.101422>
- Stavrov, O. D. 1978. Geochemistry of Lithium, Rubidium and Cesium in the Magmatic Process. M., Nedra, 216 p (in Russian)
- Steffen, D., Preusser, F., Schlunegger, F., 2009. OSL quartz age underestimation due to unstable signal components. *Quaternary Geochronology* 4, 353–362. <https://doi.org/10.1016/j.quageo.2009.05.015>
- Tabaud, A.-S., Whitechurch, H., Rossi, P., Schulmann, K., Guerrot, C., Cocherie, A., 2014. Devonian–Permian magmatic pulses in the northern Vosges Mountains (NE France): result of continuous subduction of the Rhenohercynian Ocean and Avalonian passive margin. *Geol. Soc. Lond. Spec. Publ.* 405, 197–223.
- Timar-Gabor A, Kabacinska S, Constantin D., Dave A., Buylaert J-P., 2023. Reconstructing dust provenance from quartz optically stimulated luminescence (OSL) and electron spin resonance (ESR) signals: Preliminary results on loess from around the world. *Radiation Physics and Chemistry* Viville, D., Biron, P., Granier, A., Dambrine, E., & Probst, A., 1993. Interception in a mountainous declining spruce stand in the Strengbach catchment (Vosges, France). *Journal of Hydrology*, 144:273-282. [https://doi.org/10.1016/0022-1694\(93\)90175-9](https://doi.org/10.1016/0022-1694(93)90175-9)
- Timar-Gabor, A., 2018. Electron spin resonance characterisation of sedimentary quartz of different grain sizes. *Radiation Measurements* 120, 59-65. <https://doi.org/10.1016/j.radmeas.2018.06.023>
- Tissoux, H., Toyoda, S., Falguères, C., Voinchet, P., Takada, M., Bahain, J.-J., Despriée, J., 2008. ESR Dating of Sedimentary Quartz from Two Pleistocene Deposits Using Al and Ti-Centers. *Geochronometria* 30, 23–31. <https://doi.org/10.2478/v10003-008-0004-y>



- Tissoux, H., Voinchet, P., Lacquement, F., Despriée, J., 2015. ESR as a method for the characterization of alluvial sediments. *Radiation Measurements* 81, 2–8. <https://doi.org/10.1016/j.radmeas.2015.05.010>
- Toyoda, S., Falguères, C., 2003. The method to represent ESR signal intensity of the aluminium hole center in quartz for the purpose of dating. *Advances in ESR Applications* 20, 7-10.
- 805 Toyoda, S., Ikeya, M., 1991. Thermal stabilities of paramagnetic defect and impurity centers in quartz: Basis for ESR dating of thermal history. *Geochem. J.* 25, 437-445. <https://doi.org/10.2343/geochemj.25.437>
- Toyoda, S., Ikeya, M., 1994. ESR dating of quartz with stable component of impurity centers. *Quaternary Science Reviews* 13, 625–628. [https://doi.org/10.1016/0277-3791\(94\)90089-2](https://doi.org/10.1016/0277-3791(94)90089-2)
- 810 Toyoda, S., Voinchet, P., Falguères, C., Dolo, J.M., Laurent, M., 2000. Bleaching of ESR signals by the sunlight: a laboratory experiment for establishing the ESR dating of sediments. *Applied Radiation and Isotopes* 52, 1357-1362. [https://doi.org/10.1016/S0969-8043\(00\)00095-6](https://doi.org/10.1016/S0969-8043(00)00095-6)
- Toyoda, S., Miura, H., Tissoux, H., 2009. Signal regeneration in ESR dating of tephra with quartz. *Radiation Measurements* 44, 483–487. <https://doi.org/10.1016/j.radmeas.2009.03.002>
- 815 Toyoda, S., Nagashima, K., Yamamoto, Y., 2016. ESR signals in quartz: Applications to provenance research - A review. *Quaternary International* 397, 258-266. <https://doi.org/10.1016/j.quaint.2015.05.048>
- Toyoda, S., 2015. Paramagnetic lattice defects in quartz for applications to ESR dating. *Quaternary Geochronology* 30, 498–505. <https://doi.org/10.1016/j.quageo.2015.05.010>
- Tsukamoto, S.; Nagashima, K.; Murray, A.S.; Tada, R., 2011. Variations in OSL components from quartz from Japan sea sediments and the possibility of reconstructing provenance. *Quaternary International*, 234, 182–189.
- 820 Vartanian, E., Guibert, P., Roque, C., Bechtel, F., Schvoerer, M., 2000. Changes in OSL properties of quartz by preheating: an interpretation. *Radiat. Meas.* 32, 647–652
- Wark, D.A., Watson, E.B., 2006. TitaniQ: a titanium-in-quartz geothermometer. *Contributions to Mineralogy and Petrology* 152, 743-754
- 825 Wild, B., Daval, D., Beaulieu, E., Pierret, M.-C., Viville, D., Imfeld, G., 2019. In-situ dissolution rates of silicate minerals and associated bacterial communities in the critical zone (Strengbach catchment, France). *Geochimica et Cosmochimica Acta* 249, 95–120. <https://doi.org/10.1016/j.gca.2019.01.003>
- Zular, A., Sawakuchi, A.O., Guedes, C.C.F., Giannini, P.C.F., 2015. Attaining provenance proxies from OSL and TL sensitivities: Coupling with grain size and heavy minerals data from southern Brazilian coastal sediments.
- 830 *Radiat. Meas.* 81, 39–45.



Appendix



Appendix A : Indonesian natural Quartz ESR spectra with similar Ti centers intensities (a.u.) higher than Al centers intensities (HNHP data, 2019)

835



Appendix B: Pictures of the rocks samples and outcrops from Strengbach catchment (France)

840



Sample	Li	+/-	LOD max	Ti	+/-	LOD max	Al	+/-	LOD max
STR22_01	2,17	0,51	0,92	22,22	5,39	1,72	57,97	28,01	5,99
STR22_02	2,79	1,26	0,96	37,10	8,38	1,76	122,00	61,26	5,7
STR22_09A	3,73	2,86	3,77	29,55	17,38	3,17	105,13	23,45	5,28
STR22_09B	6,77	2,65	1	18,99	12,67	2,38	101,74	20,07	6,61
STR22_10	5,12	3,23	4,01	22,39	6,01	3,13	100,55	17,54	5,48
STR22_14	<4.01	<i>n.d.</i>	4,17	16,26	2,00	3,18	85,14	15,62	4,29
STR22_15	16,38	3,79	3,84	36,06	7,28	5,83	140,38	26,07	2,88
STR22_17	6,04	2,23	1,04	31,16	2,69	2,32	74,97	14,17	8,29
STR22_20	21,18	3,48	3,73	35,44	10,19	2,98	187,56	13,30	4,61
STR22_30	15,63	3,98	2,02	44,23	9,60	2,33	137,03	44,48	6,25
STR22_32	4,72	0,70	3,94	48,42	5,34	3	73,43	8,77	4,39
STR22_33	0,92	0,61	3,74	35,62	4,92	3,01	72,66	30,34	4,66
STR22_44	8,16	3,79	1,05	31,14	13,93	1,79	163,69	80,64	5,92
STR22_45	30,27	2,46	3,51	41,05	5,91	2,89	219,86	8,88	4,15
STR22_29	18,15	7,34	0,89	27,19	12,77	1,76	176,32	72,08	5,14

Appendix C : Li, Ti and Al mean content (ppm) with maximal limit of detection (LOD) obtained by LA-ICP-MS for the rocks of the Strengbach catchment (France)

845